# Statistical analysis of rain fade slope

# Statistical Analysis of Rain Fade Slope

Max M. J. L. van de Kamp

***Abstract*—An analysis is made of the measured distributions of the fade slope of rain attenuation, conditional for attenuation values, measured at Eindhoven University of Technology from the satellite Olympus. It is found that the distribution is similar for positive and negative fade slopes and independent of frequency in the range from 12 to 30 GHz. A distribution model for the conditional distribution is found. The only parameter of the distribution is the standard deviation, which is found to be proportional to attenuation level and dependent on rain type, on the low-pass filter bandwidth and on the time interval used in the slope calculation. The observed relation between the standard deviation and attenuation is compared with results from other measurement sites. From this comparison it is found that the fade slope standard deviation is likely to depend on elevation angle and on climate, through its dependence on rain type.**

***Index Terms*—Adaptive fade countermeasures, fade slope, microwave propagation, rain, rain attenuation, satellite communications, up-link power control.**

## I. Introduction

THE statistical aspects of rain attenuation on microwave links have already widely been measured and studied. This paper concentrates on a particular dynamic aspect: the rate of change of rain attenuation or "fade slope." Information about the maximum fade slope to be expected is important, e.g., for the design of adaptive fade countermeasures.

A common fade countermeasure system is open-loop up-link power control (ULPC), in which the attenuation on a satellite uplink is estimated from the attenuation measured on the downlink by frequency scaling and compensated by increasing the transmitted power on the uplink e.g., [1]. Information about the fade slope to be expected is hereby essential to assess the required minimum tracking speed of a ULPC system.

Sweeney and Bostian [2] theoretically examined the dynamics of rain-induced fades by evaluating the rate at which the first Fresnel zone volume fills with rain. Their analysis, although it neglects many important influences, gives useful insight into the physics of fade changes. The main conclusion is that there is no deterministic relation between attenuation and fade slope, because the latter depends on other stochastic parameters and varies with time. Therefore, instead of a deterministic relation, in this paper the probability distribution of fade slope will be studied and its dependencies assessed.

Buné, Herben, and Dijk [3] analyzed the physical dynamic behavior of rain events. They started from an assumed attenuation event, during which the fade slope depends on attenuation level similarly as found by Matricciani [4]. Assuming a cylindrical rain cell which would be moved across the propagation path by wind, they then looked for a rain intensity profile which would correspond to this attenuation record. A rain rate profile which agrees with meteorological measurements from other sources appeared to give a good fit. Furthermore, they found from their measured attenuation data that at least about half of the events corresponded well with the assumed attenuation record they started with.

From these analyses is found that the fade slope probability distribution is likely to depend on climatic parameters. Due to the dependence on attenuation and on rain rate profile, the fade slope will depend on the drop size distribution and therefore on the type of rain. A convective rainstorm may cause different fade slopes than a widespread rainstorm. The horizontal wind velocity perpendicular to the path is another climatic parameter of influence, determining the speed at which the horizontal rain profile passes across the propagation path.

Both analyses were made under the assumption of one rain cell with a certain rain rate profile. If more rain cells and/or different kinds of rain can be present, the fade slope is likely to decrease with path length. A certain attenuation level on a longer path is more likely to be caused by widespread rain, or by several rain cells integrated over a longer distance, while the same attenuation on a shorter path is more likely to be due to a single, more intense rain cell. The widespread rain or combination of rain cells on the longer path is less likely to change rapidly than the single rain cell. It can be concluded that the expected fade slope at a given attenuation level is likely to decrease with path length and therefore increase with elevation angle on satellite links.

Summarizing, it is expected that the fade slope depend on the following climatic parameters:

- attenuation level;
- drop size distribution;
- rain type (widespread/convective);
- (horizontal) wind speed;
- path length (through rain).

Furthermore, the measured fade slope is likely to be influenced by dynamic parameters, or time constants, of the receiving system. A receiver with a longer integrating time is likely to reduce the instantaneous fade change and spread it out over a longer period of time.

In this paper, several properties of the fade slope will be analyzed using measurement results from Eindhoven [5], [6].

## II. Measurement Analysis

### A. Measurement Results

The beacon signals from the satellite Olympus, at 12.5 GHz, 20 GHz (dually polarized) and 30 GHz, were received and an-

Manuscript received January 5, 2000; revised March 19, 2001.

The author was with Eindhoven University of Technology, EH 11.09, P.O. Box 513, 5600 MB Eindhoven, the Netherlands. He is now with ONERA/DEMR, P.O. Box 4025, 31055, Toulouse, CEDEX 4, France.

Digital Object Identifier 10.1109/TAP.2003.808542

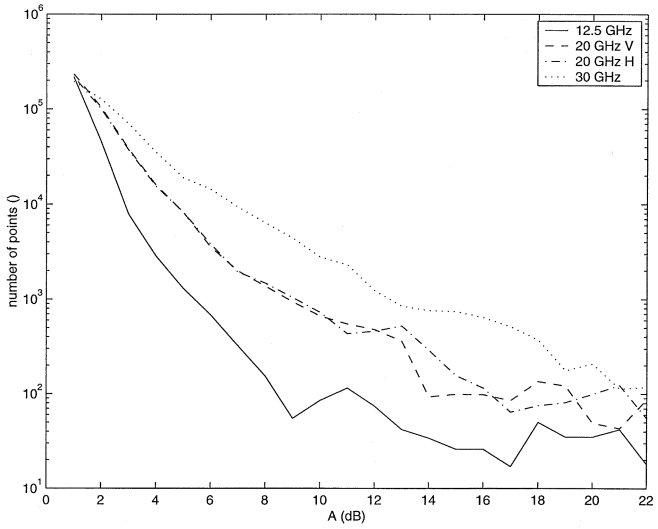


Fig. 1. Number of data points (seconds) in the data base for each attenuation value and each beacon signal.

alyzed at Eindhoven University of Technology. Fade slope statistics were generated from 104 attenuation events, measured between January 1991 and June 1992. The attenuation during the events had been sampled at a frequency of 3 Hz and averaged over every second. The elevation angle of Olympus seen from Eindhoven was 26.8°.

For the fade slope analysis, the attenuation data were low-pass filtered to remove fluctuations due to tropospheric scintillation. The optimum filter bandwidth was determined from the power spectrum of the signal variations, as the threshold frequency between the attenuation spectrum, which decreases with frequency, and the flat part of the scintillation spectrum. The value of this threshold frequency varies from event to event, but a value of 20 mHz was found as a lower limit. A filter bandwidth $f_B$ of 20 mHz was therefore used, which is expected to effectively remove the scintillations.

Inevitably, the low-pass filter will also remove attenuation variations with time periods shorter than 1/20 mHz $=$ 50 s. This is likely to affect the fade slope results; this subject is addressed in Section II-E.

In Fig. 1, the numbers of data points (seconds) for each attenuation value and for each beacon signal are shown. As can be expected, the amounts of data decrease with attenuation and for a given attenuation increase with frequency. This will be important information for an accuracy evaluation, as given in Section II-C.

For each sample the fade slope $\zeta$ was calculated as

$$\zeta(i) = \frac{A(i+1) - A(i-1)}{2} \quad \text{(dB/s)} \tag{1}$$

where $A$ is attenuation and $i$ is the sample number. Joint statistics of $\zeta$ and $A$ were generated for each beacon signal. The sizes of the bins were 0.001 dB/s for $\zeta$ and 1 dB for $A$.

In Fig. 2, the conditional probability densities are shown for the fade slope $\zeta$, for $A$ in the bins 1, 2,… 5 dB. This figure shows that the fade slope is always distributed around 0 dB/s and has a spread which increases with attenuation. Furthermore, the distributions are very similar for the different beacons, even though the samples were very differently distributed over the attenuation bins for the three frequencies. This suggests that the conditional distribution of $\zeta$ for a certain value of $A$ is independent of frequency. This point will be addressed more quantitatively in Section II-C.

Some properties of these distributions will be studied and a model for the distribution will be formulated in the following sections.

### *B. Time Symmetry*

Fig. 2 shows that the distributions are very similar for positive and negative fade slopes. The same was observed for the other attenuation bins. In order to check this quantitatively, some parameters were calculated from the distributions: the median slope values and the average positive and negative slopes.

No substantial deviation of the median value from zero was found. When varying $A$ from 1 to 12 dB, the median divided by the standard deviation fluctuated, positively as much as negatively, between $-0.1$ and $+0.1$, with an average between $-0.03$ and $+0.03$, depending on the frequency. Similar calculations were made for subsets of data, using only the events with peak attenuation below or above certain threshold values, in order to separate the stratiform and convective rain events. The threshold attenuation used was varied from 1 to 20 dB. Also here, no substantial deviation of the median value from zero was found in either direction, for any threshold value.

Another indicator of asymmetry of the distribution could be the difference between the average positive slopes and the average negative slopes. However, also here no sign of asymmetry was observed. The average positive slope was larger than the average negative slope in 54% of the cases, for $A \leq 20$ dB. The relative difference between the average positive and negative slopes was almost always between $-15\%$ and $+15\%$. Similar results were again found from subsets of data with peak attenuation below and above various thresholds.

It is thus found that the measurements show no sign of asymmetric behavior of the fade slope distribution, either for the whole database or for only low- or high-attenuation events. This shows that on a statistical basis, attenuation events are symmetrical. This result was also found by other experimenters [3], [4], [7], [8].

### *C. Attenuation Dependent Distribution Model*

For the conditional distribution of fade slope $\zeta$ for fixed values of attenuation $A$ (shown in Fig. 2), a reasonable fit was found with the following model distribution

$$p(\zeta|A) = \frac{2}{\pi\sigma_\zeta \left(1 + \left(\frac{\zeta}{\sigma_\zeta}\right)^2\right)^2} \quad ((\text{dB/s})^{-1}). \tag{2}$$

This distribution is symmetrical around zero. Its mean value is (consequently) 0 dB/s and the only characterising parameter

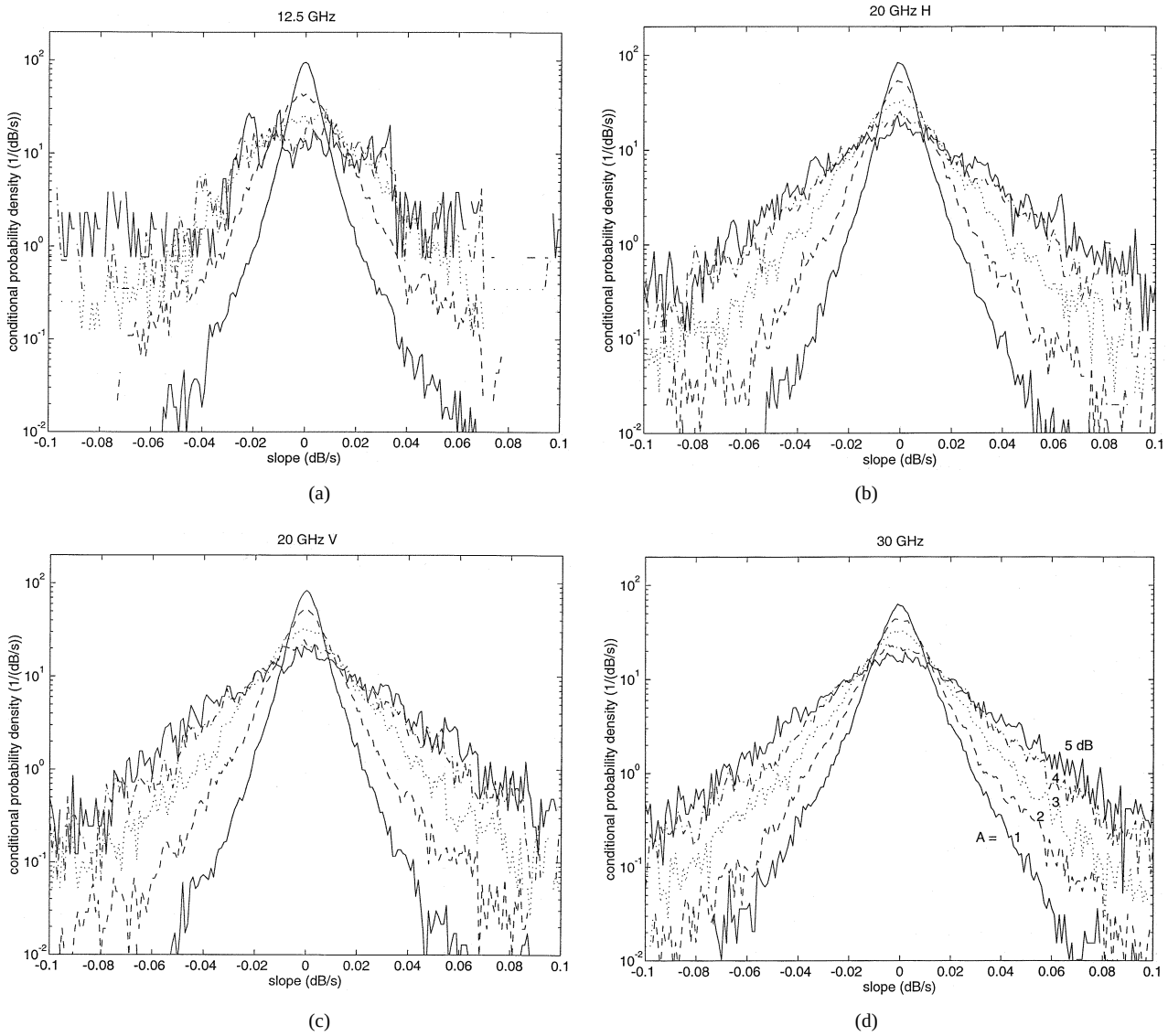


Fig. 2. Conditional distribution of fade slope $\zeta$ for $A$ in the bins specified in the lower right graph, at 12 GHz (a); 20 GHz H (b), 20 GHz V (c) and 30 GHz (d).

is $\sigma_\zeta$, the standard deviation of $\zeta$. Compared to a Gaussian distribution with the same standard deviation, the distribution of (2) has higher tails and a higher, sharper peak. In Fig. 3, the distribution is shown for different values of $\sigma_\zeta$.

Comparing Fig. 3 with Fig. 2 it can be seen that the distribution of $\zeta$ for any fixed $A$ value can be approximated by (2), with $\sigma_\zeta$ as the only characterising parameter and that $\sigma_\zeta$ is dependent on $A$. To find the relation between these, the value of $\sigma_\zeta$ was calculated from the conditional distribution of $\zeta$ for every $A$-bin, for every beacon signal. In Fig. 4, the results are shown as a function of $A$. This figure shows that $\sigma_\zeta$ is approximately proportional to $A$ and that the relation of $\sigma_\zeta$ with $A$ is very similar for all frequencies.

In Fig. 4, the fluctuating results for attenuation values above about 8 dB are caused by a decreasing accuracy in the calculation of the standard deviation, due to the decreasing number of data points, shown in Fig. 1. This effect is strongest at 12.5 GHz, because the number of samples for large attenuation values is smallest at this (lowest) frequency.

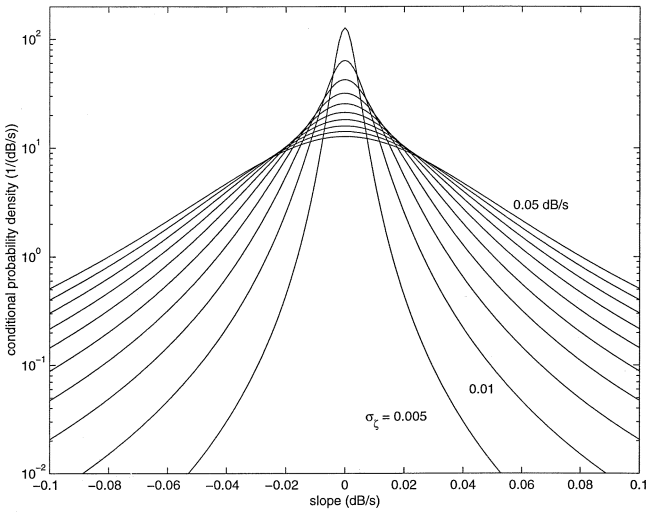


Fig. 3. Modeled conditional distribution of fade slope $\zeta$, with $\sigma_\zeta = 0.005$, 0.01, 0.015,…, 0.05 dB/s.

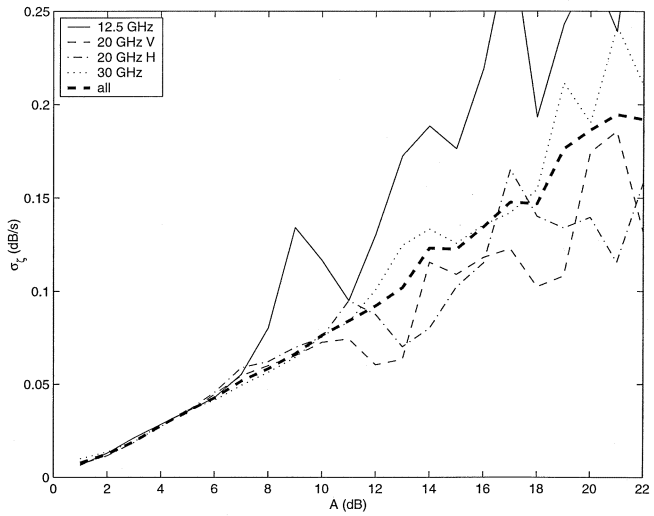


Fig. 4. $\sigma_\zeta$ as a function of $A$ for each of the beacon signals and for all beacons together (thick dashed line).

An accuracy evaluation of the calculation of $\sigma_\zeta$ is made as follows. The rms relative error of a standard deviation calculated from a sample distribution is given by [9]

$$\frac{rms\,(\sigma_\zeta)}{\sigma_\zeta} = \frac{1}{\sqrt{2(N-1)}} \tag{3}$$

where $N$ is the number of samples in the distribution from which the standard deviation is calculated. Using this formula and the numbers of data points shown in Fig. 1, is found that the rms relative error of $\sigma_\zeta$ in Fig. 4 increases with $A$ and decreases with frequency. For $A = 8$ dB, at 12.5 GHz ($N = 154$) the error is 6%, at 20 GHz ($N = 1475$ and 1372) 2% and at 30 GHz ($N = 6381$) 1%. Since the relative error is even smaller for smaller $A$, this indicates that the conclusion from Fig. 4 that $\sigma_\zeta$ is proportional to $A$, is justified.

The theoretical frequency dependence of the fade slope distribution can also be estimated. According to the ITU-R [10], rain attenuation statistics can be scaled in frequency in the range 7 to 55 GHz by the formula

$$\frac{A_2}{A_1} = \left(\frac{b_2}{b_1}\right)^{(1-1.12\times10^{-3}\sqrt{b_2/b_1}(b_1A_1)^{0.55})} \tag{4}$$

where

$$b_i = \frac{f_i^2}{1+10^{-4}f_i^2} \tag{5}$$

and $f$ is the frequency in GHz. According to (4), the ratio between equiprobable attenuations $A_2$ and $A_1$ at 30 and 20 GHz is almost constant: with $A_1$ at 20 GHz varying from 1 dB to 20 dB, this factor varies from 2.07 to 1.81. Similarly, the ratio between equiprobable attenuations at 12.5 and 20 GHz varies from 0.41 to 0.44. This means that the distribution of $A_1$ at one frequency is almost proportional to that of $A_2$ at another.

Furthermore, instantaneous $A$ values at two frequencies are generally found to be not perfectly, but reasonably, correlated e.g., [11]. Because of this, also the instantaneous $A_1$ and $A_2$ are approximately proportional. This property is already used in many fade countermeasure systems, where the attenuation at one frequency is estimated from that at the other e.g., [1]. This property can be expressed by a scaling factor

$$A_2 = aA_1 \tag{6}$$

which is approximately true for each separate sample and for each frequency pair $f_1$ and $f_2$. From (1) it follows that then also

$$\zeta_2 = a\zeta_1 \tag{7}$$

is approximately true for every separate sample. The standard deviation $\sigma_{\zeta 1}$ of the distribution of $\zeta_1$ at $f_1$ conditional for $A_1$ must then also be proportional to $\sigma_{\zeta 2}$ of the distribution of $\zeta_2$ at $f_2$ in the same portion of time, i.e., conditional to $A_2$

$$\sigma_{\zeta 2} = a\sigma_{\zeta 1}. \tag{8}$$

In Fig. 4, $\sigma_\zeta$ was found to be approximately proportional to $A$ for all frequencies

$$\sigma_{\zeta 1} = s_1A_1 \qquad \sigma_{\zeta 2}s_2A_2. \tag{9}$$

It follows easily from (6), (8) and (9) that the proportionality factors $s_1$ and $s_2$ must be the same. It thus follows that if the conditional fade slope distribution $p(\zeta|A)$ is proportional to $A$, it must be independent of frequency in the range 12 to 30 GHz, even though the rainy conditions which cause a certain attenuation $A$ are very different for different frequencies.

This is in agreement with Figs. 2 and 4, where no significant difference between the results of different frequencies was found. Also Feil, Ippolito Jr., Helmken, Mayer, Horan and Henning [8] observed from measurements from the ACTS-satellite at several ground stations in the US, that the probability of the fade slope at a given fade level was very similar for 20 and 27 GHz. Of course, the total distributions of fade slope may still be frequency dependent, due to frequency dependence of the attenuation statistics.

In order to increase the amount of data per $A$-bin, the distributions of $\zeta$ for all four beacon signals were put together in one distribution for each bin and the standard deviations were again calculated. The result, as a function of $A$, is also included in Fig. 4 (thick dashed line). The result is obviously more stable than the curves for the different beacons and confirms that $\sigma_\zeta$ is approximately proportional to $A$ for the analyzed data set from the ground station in Eindhoven. Later, this result will be compared to results from other measurement sites.

### *D. Dependence on Rain Type*

As discussed earlier, the fade slope depends on horizontal wind velocity and drop size distribution and its distribution is therefore likely to be climatic dependent and dependent on the type of rain. In particular, in a convective rainstorm the rain intensity can be expected to change suddenly by large steps, while in stratiform rain it varies more gradually, even though the average intensity may be equal to that of the convective storm.

It was studied whether this difference in typical behavior has any effect on the fade slope distribution, in the following way. The database was divided in events with peak event attenuation below certain thresholds, in order to isolate stratiform rain and above certain thresholds, in order to isolate convective rain. The attenuation at 30 GHz (after low-pass filtering) was used in this criterion. The attenuation threshold was varied from 1 to 20 dB.

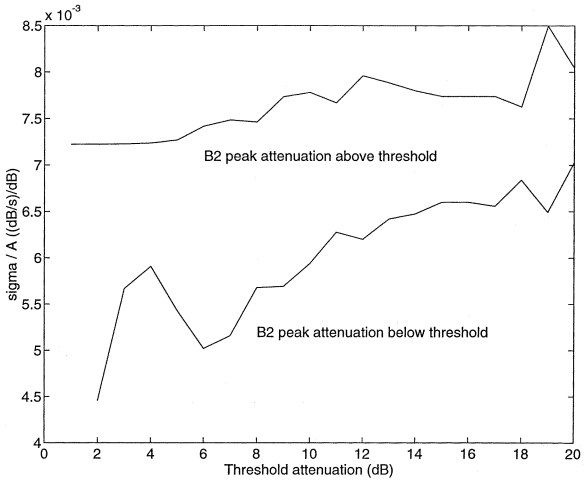


Fig. 5. $\sigma_\zeta/A$ for selections of the database with events with peak attenuation at 30 GHz above and below different threshold values.

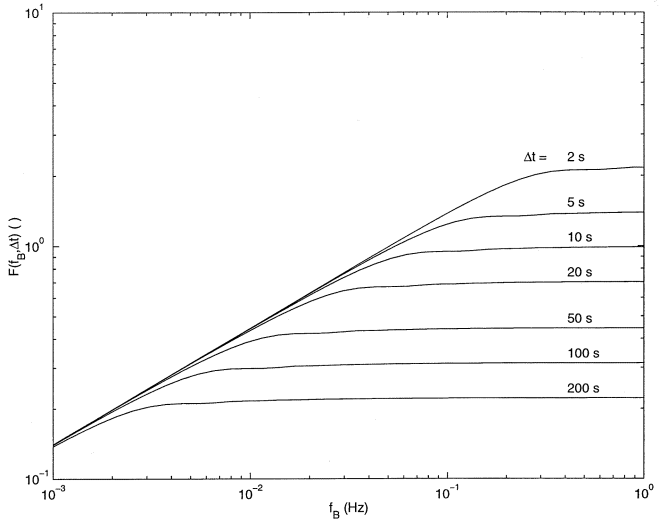


Fig. 6. $F(f_B, \Delta t)$ versus filter bandwidth $f_B$, for different time interval lengths $\Delta t$.

The numbers of events in both groups varied with the attenuation threshold: at a threshold of 1 dB, all of the 104 events were classified as 'convective'; at 10 dB, 37 events; at 15 dB, 18 events; and at 20 dB, 10 events. The dependence of $\sigma_\zeta$ on $A$ was again determined for each data selection; these all again appeared to be approximately proportional. The coefficient $\sigma_\zeta/A$ was determined for each case and the results are shown in Fig. 5.

This figure shows that $\sigma_\zeta/A$ significantly decreases if only the light events are selected and increases slightly when only heavy events are selected. This means that the conditional fade slope standard deviation is smaller for light rain events than for heavy rain events, for equal $A$-values. This is a first indication that the fade slope distribution is dependent on rain type. No quantitative conclusions can yet be drawn from this result, because events of the two rain types were probably not completely separated. It is impossible to effectively detect stratiform or convective rain using only the peak event attenuation. Nonetheless, this qualitative conclusion is useful when the results of Eindhoven are compared to those from other sites and climatic dependencies are considered.

### *E. Dependence on Filter Bandwidth and Time Interval*

There is reason to expect that the fade slope distribution is dependent on low-pass filter ('LPF') bandwidth and on the time interval between the samples used for the slope calculation.

Matricciani [12] performed experiments with fade slope statistics, measured from the satellite SIRIO at the ground station of Gera Lario, Italy. Scintillation effects were removed by low-pass filtering the data with two moving-average filters with different time periods: 1 s and 4 s, in order to compare the results. From these two analyzes, he found distributions of similar shapes, apart from a multiplication factor: the fade slope exceeded for the same probability was significantly larger for the larger filter bandwidth. He explained this by the smoothing and resampling which causes longer rising and sinking times over a given attenuation interval. If the same effect is true for other measurements, the results of the previous section should also be dependent on the bandwidth $f_B$ of the filter used.

Maseng and Bakken [13] derived a theoretical model for the dynamic behavior of rain attenuation. From the result it can be seen that for small time intervals $\Delta t$ between two attenuation samples, the standard deviation of the second one, given the first one is known, increases proportionally to $\sqrt{\Delta t}$. If the fade slope $\zeta$ is calculated as the difference between these two values divided by the time interval $\Delta t$ between them (as in (1), where $\Delta t$ is 2 s), it can be calculated that its standard deviation $\sigma_\zeta$ is proportional to $1/\sqrt{\Delta t}$.

However, neither of these dependencies is likely to be uniformly valid. If the fade slope is calculated between two samples with a time interval $\Delta t$ between them much larger than the inverse of the filter bandwidth $f_B$, the LPF will not affect attenuation changes over the time $\Delta t$, so the fade slope standard deviation $\sigma_\zeta$ will not depend on $f_B$. On the other hand, if $\Delta t$ is much smaller than $1/f_B$, then on a time scale of the order of $\Delta t$, the filtered signal will show no sudden changes. In this situation the calculated fade slope is the time derivative of attenuation, regardless of the exact length of $\Delta t$. The instantaneous fade slope will then be independent of $\Delta t$ and so will its standard deviation $\sigma_\zeta$.

In order to quantify the dependence of fade slope standard deviation on filter bandwidth and time interval, van de Kamp and Clérivet [14] showed that the conditional fade slope standard deviation is proportional to the following expression:

$$\sigma_\zeta \propto F(f_B, \Delta t) = \sqrt{\frac{2\pi}{\Delta t}\int_0^{\pi f_B \Delta t}\left(\frac{\sin x}{x}\right)^2 dx} \qquad (10)$$

where $f_B$ is the LPF bandwidth (Hz) and $\Delta t$ is the time interval (s). This function is plotted in Fig. 6. For $f_B\Delta t \gg 1$, $F(f_B, \Delta t)$ can be approximated by $\pi/\sqrt{\Delta t}$ and for $f_B\Delta t \ll 1$, by $\pi\sqrt{2f_B}$.

The filtering method in this analysis and in the data processing in Eindhoven, had been to sharply cut off all frequency components above $f_B$. However, in many other fade slope analysis procedures, moving-average filters are used. These filters replace each sample by the average of the samples in the block of length $t_a$ around it. In order to compare the effects of these filters, a selection of data was processed using sharp filters with bandwidths from 0.5 to 500 mHz and moving-average filters

with averaging times from 2 to 2000 s. It appeared that the results were very similar when an effective filter bandwidth for moving-average filters is defined as

$$f_B = \frac{0.445}{t_a}. \tag{11}$$

The same test was performed for so-called $\cos^2$-filters. This type of filter is similar to a moving-average filter, but before averaging it multiplies the samples in the block by a $\cos^2$-shaped function, with the nulls at the edges and the maximum in the center. This action removes all discontinuities from the signal. From this test, it was found that an effective filter bandwidth for $\cos^2$-filters is given by

$$f_B = \frac{0.719}{t_a} \tag{12}$$

It can be concluded that the dependence of $\sigma_\zeta$ on filter bandwidth for any LPF filter is expressed by (10). For moving-average filters and $\cos^2$-filters, the effective signal bandwidth can be calculated from (11) and (12). It should also be noted that using large filter bandwidths (from about 100 mHz), the result is likely to contain tropospheric scintillation.

## III. Comparison With Other Sites

Fade slope has also been measured and analyzed at many other experimental sites and the results of some of these studies have been published in literature. Also, measured rain attenuation data from several experimental sites have been submitted to ONERA, Toulouse, France, where fade slope statistics have been analyzed from them. In this section, some of these results are compared to the results from Eindhoven, in order to assess the influence of other parameters than those discussed in the previous sections.

Statistical results of fade slope from publications are considered only where these are given specifically for different attenuation levels. This is because, as was seen above, the distribution of fade slope depends strongly on the attenuation statistics. Comparison of the total distribution between different sites would therefore be very complicated.

Experimental results from 12 sites were collected [7], [8], [15]–[19]. In Table I, parameters of the measurement sites are given. Some details on the data processing procedures at the different measurement sites are given in the Appendix. In the publications, the measurement results are usually presented in graphs. The information has been extracted from these by enlarging the paper copies and scanning the graphs by hand. This way, an estimated accuracy of $\approx 0.1\%$ of the maximum range of the graphs could be reached.

The standard deviation $\sigma_\zeta$ was estimated from the published distributions as follows. The theoretical relation between the standard deviation $\sigma_\zeta$ and the probability of samples in each bin was calculated from the model distribution (2). By inverting this relation, $\sigma_\zeta$ could be estimated from each bin content of the measured distributions. This was done for all of the reported conditional fade slope distributions. In most cases, the resulting $\sigma_\zeta$ was similar for all bins of a distribution, which indicates that (2) is a good estimate of the measured distributions. The few outlying values were removed and the calculated $\sigma_\zeta$ was averaged over each distribution.

TABLE I
Site Parameters of the Measurements of Fade Slope Distribution: Site Names, Coordinates, Frequencies $f$, Elevation Angles $\varepsilon$, LPF Specifications, Time Intervals $\Delta t$, and Satellite Names

| ground station | coord. | $f$ (GHz) | $\varepsilon$ (°) | LPF | $\Delta t$ (s) | satellite |
|---|---|---|---|---|---|---|
| Blacksburg, Virginia [7] | 37.23 - 279.60 | 12.5 19.8 29.7 | 14 | 10s mov. av. | 10 | Olympus |
| Chilton, UK [15] | 51.57 - 358.72 | 29.7 | 28.6 | 10s mov. av. | 10 | Olympus |
| Fairbanks, Alaska [8] | 64.86 - 212.18 | 20.2 27.5 | 8.1 | 100s $\cos^2$ | 10 | ACTS |
| Gometz-la-Ville, France [16] | 48.67 - 2.12 | 19.8 29.7 | 30.3 | 40s $\cos^2$ | 2 | Olympus |
| La Folie Bessin, France [16] | 48.67 - 2.20 | 19.8 29.7 | 30.3 | 40s $\cos^2$ | 2 | Olympus |
| La Salle, Colorado [17] | 40.35 - 255.28 | 20.2 27.5 | 43 | 10s mov. av. | 10 | ACTS |
| Lessive, Belgium [18] | 50.22 - 5.25 | 12.5 19.8 | 27.6 | 20 mHz sharp | 2 | Olympus |
| Louvain-la-Neuve, Belgium [18] | 50.67 - 4.62 | 12.5 29.7 | 27.8 | 20 mHz sharp | 2 | Olympus |
| Sparsholt, UK [15] | 51.07 - 358.57 | 19.8 | 29.2 | 10s mov. av. | 10 | Olympus |
| Sparsholt, UK [19] | 51.07 - 358.57 | 18.7 | 29.9 | 40s $\cos^2$ | 2 | Italsat |
| Tampa, Florida [8] | 28.06 - 277.58 | 20.2 27.5 | 52.1 | 100s $\cos^2$ | 10 | ACTS |
| White Sands, New Mexico [8] | 32.37 - 253.62 | 20.2 27.5 | 51.5 | 100s $\cos^2$ | 10 | ACTS |

The measurement sites involved in the ACTS-project had a particular problem: a water-absorbing antenna coating which during rain events caused an extra attenuation of up to 3 dB at 20.2 GHz and up to 5 dB at 27.5 GHz [20]. In general, it can be expected that once the antennas had gotten wet, the attenuation caused by this effect was relatively constant during the rain events. Because of this, the fade slope will not have been affected very much, but the concurrently measured attenuation was a few dB higher than that caused by rain alone. In the online ACTS-database (http://rossby.metr.ou.edu/~actsrain/), correction values are provided to compensate attenuation distributions for this effect. The fade slope distributions used in this study have been corrected, by adjusting the $A$ bin values according to these correction values.

Comparing the results from all of the sites, it appeared that the values of $\sigma_\zeta$ were not significantly different for different frequencies, similarly as found from the Eindhoven results. This confirms once more that $\sigma_\zeta$ does not depend on frequency in the frequency range considered. The resulting values from the different frequencies were averaged for each $A$-value.

As was found in the previous section, $\sigma_\zeta$ depends strongly on the filter bandwidth and time interval used in the data processing. In order to compare the different results, the values of $\sigma_\zeta$ were normalized by dividing them by $F(f_B, \Delta t)$ from (10), where $\Delta t$ is the time interval and $f_B$ is the LPF bandwidth, which was estimated using (11)–(12), depending on the type of filter.

In Fig. 7, the normalized standard deviations from all of the reported sites are plotted as functions of $A$. This figure shows,

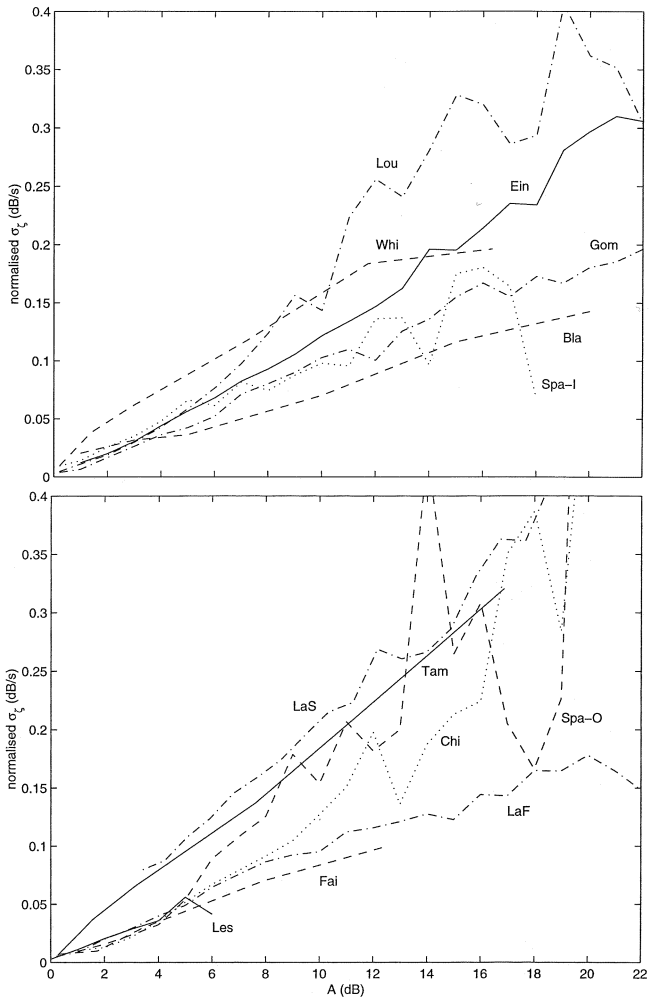


Fig. 7. Normalized $\sigma_\zeta$ as a function of $A$ for the different stations (each one indicated by the first three letters of the name; 'O' = Olympus; 'I'= Italsat). The separation into two graphs is simply for a clearer view.

that although for all sites $\sigma_\zeta$ increases with $A$, some significant differences remain. For each station, the normalized $\sigma_\zeta$ can be approximated as proportional to $A$

$$\sigma_\zeta = SF(f_B, \Delta t)\, A \quad \text{dB/s.} \tag{13}$$

The value of the coefficient $S$ was determined for each station by fitting zero-offset straight lines to the curves of Fig. 7. The results of this are:

| | $s$ |
|---|---|
| Blacksburg | 0.0074 |
| Fairbanks | 0.0082 |
| Gometz-la-Ville | 0.0093 |
| La Folie Bessin | 0.0098 |
| Lessive | 0.0102 |
| Sparsholt—Italsat | 0.0103 |
| Louvain-la-Neuve | 0.0110 |
| Chilton | 0.0110 |
| Eindhoven | 0.0136 |
| Sparsholt—Olympus | 0.0160 |
| White Sands | 0.0162 |
| Tampa | 0.0188 |
| La Salle | 0.0208 |

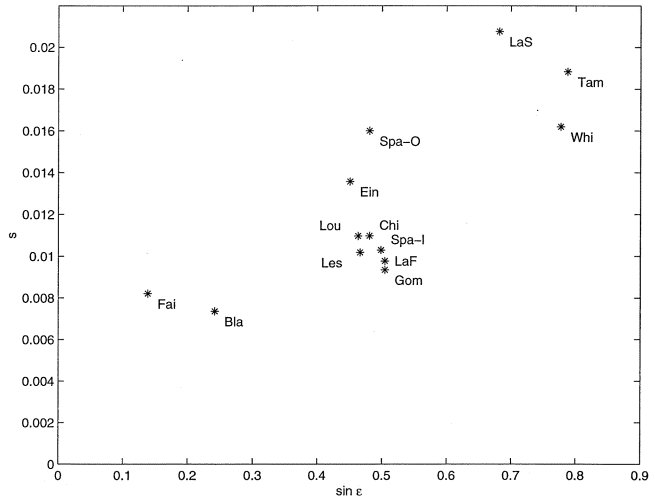


Fig. 8. The correlation of the parameter $S$ with sin $\varepsilon$.

Feil *et al.* [8] explained the different result from Fairbanks from those from Tampa and White Sands by suggesting that the fade slope distribution is dependent on elevation angle. This seems plausible, considering that lower elevation links have a longer path length through rain. As discussed before, a certain attenuation level on a longer path, being more likely caused by widespread rain or several rain cells, is less likely to change rapidly than the same attenuation on a shorter path, more likely caused by a single rain cell. A parameter expressing the influence of the elevation angle $\varepsilon$ by the expected dependence on path length is sin $\varepsilon$, which is proportional to the path length through rain (if the rain height is constant). In Fig. 8, the parameter $S$ is shown for all sites versus sin $\varepsilon$.

Fig. 8 indeed seems to indicate an elevation dependence: both $S$ and sin $\varepsilon$ are relatively low in Fairbanks and Blacksburg and relatively high in la Salle, White Sands and Tampa. On the other hand, in Blacksburg $S$ is lower than in Fairbanks and in la Salle higher than in White Sands and Tampa. This indicates that there may be other influencing parameters than the elevation angle.

Earlier, it was discussed that, because of the influence of drop size distribution and wind velocity, the distribution of fade slope may be climate dependent. An explanation of the differences may then be found from the climatic characteristics of the measurement sites, according to the Köppen classification [21]. In northwestern Europe (Marine West Coast Climate), rain is usually of the widespread type, while in la Salle (Middle-Latitude Steppe), White Sands (Subtropical Steppe) and Tampa (Humid Subtropical Climate) convective rain prevails. This suggests that convective rain causes higher fade slopes than widespread rain for similar attenuation values, which is in agreement with an earlier conclusion. Also in Fairbanks (Subarctic Climate) the rare rain is usually convective, but $S$ is relatively low. This may be due to the low elevation angle, which indicates that the elevation angle also has some influence. Blacksburg is, according to Köppen, in the same climatological region as Tampa, but its $S$ is lower. This can be due both to the lower elevation angle and to the more northerly location, causing the site to experience more middle-latitude cyclone fronts with widespread rain than Tampa.

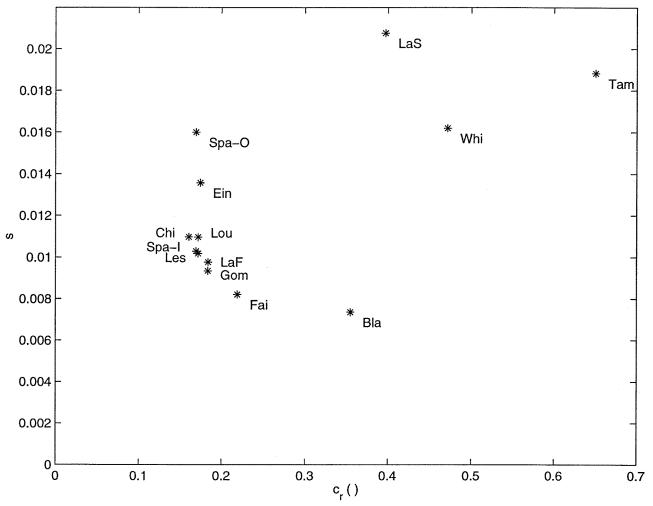


Fig. 9. The correlation of the parameter $S$ with the convectivity of rain $C_r$.

A meteorological parameter which expresses the prevalence of convective rain was provided by J. Pedro V. Poiares Baptista of ESTEC. This parameter $C_r$, the convectivity of rain, represents the average amount of convective rainy time relative to the total rainy time. It was given in a global matrix with a spatial resolution of 1.5° both in latitude and longitude. The value of $C_r$ for the sites considered here was calculated by two-dimensional linear interpolation between the four nearest grid points. The results of this are:

| | $C_r()$ |
|---|---|
| Blacksburg | 0.355 |
| Fairbanks | 0.219 |
| Gometz-la-Ville | 0.184 |
| La Folie Bessin | 0.184 |
| Lessive | 0.172 |
| Sparsholt—Italsat | 0.170 |
| Louvain-la-Neuve | 0.172 |
| Chilton | 0.161 |
| Eindhoven | 0.175 |
| Sparsholt—Olympus | 0.170 |
| White Sands | 0.471 |
| Tampa | 0.650 |
| La Salle | 0.397 |

In Fig. 9, the parameter $S$ is shown versus the rain convectivity $C_r$. This figure shows a significant correlation in some, but not in all cases. In particular, in la Salle $S$ is much larger than in Blacksburg, while $C_r$ is almost equal in those two places.

Since both parameters sin $\varepsilon$ and $C_r$ show partially a good correlation with $S$, it might be expected that using a combination of the two, all differences between the results may be explained and a global prediction model of the fade slope distribution may be developed. Unfortunately, this appears not possible. The cases with poor correlation between $S$ and sin $\varepsilon$ (Blacksburg vs. Fairbanks; and La Salle vs. Tampa and White Sands) also show a poor correlation between $S$ and $C_r$. The inclusion of $C_r$ in addition to sin $\varepsilon$ does therefore not improve the predictability of $S$.

It can thus be concluded that $S$ is probably dependent on $\varepsilon$ and on $C_r$ or another parameter expressing the convectivity of rain, but the exact form of this dependence remains as yet unclear. $S$ is lowest in the Subarctic and Marine West Coast climates and highest in Steppe and Subtropical climates. It is also possible that geographical parameters (coast/desert/mountains) influence the local behavior of rainstorms and thereby the fade slope distribution. The search for meteorological or geographical parameters which can explain the differences in $S$ and form with (13) a prediction model of $\sigma_\zeta$, remains a subject for further study.

## IV. Conclusion

The long-term probability distribution of fade slope $\zeta$, for a certain value of attenuation, is similar for positive and negative fade slopes, independent of frequency in the range from 12 to 30 GHz, but dependent on filter bandwidth and time interval. For a given fixed link it only depends on rain type and attenuation level. The conditional distribution can be approximated by (2). The only parameter of this distribution is the standard deviation $\sigma_\zeta$, which for a given link is approximately proportional to attenuation $A$. It can be approximated by (13). The coefficient $S$ in this equation is independent of frequency, but differs for different rain types and also between different sites. It is likely to depend on elevation angle and on climate. Results from several sites indicate that $S$ is lowest for the Subarctic and Marine West Coast climate and highest for Steppe and Subtropical climates.

## V. Remarks W.r.t. Adaptive Fade Countermeasures

The results obtained in this paper are important steps in the development of a model to predict rain fade slope from attenuation statistics or from momentary attenuation values. This information is useful to assess the minimum speed with which a fade countermeasure system should be able to track changes in rain attenuation.

As this paper addresses only the effects of rain, the results obtained are applicable to the compensation of rain attenuation, not of signal fluctuations due to scintillation. The results can be used e.g., in a ULPC system where the downlink signal is low-pass filtered and only this low-frequency component on the uplink is estimated and compensated. Since in the frequency range considered, signal fades due to scintillation are much smaller than those due to rain, typically up to only a few dB, ignoring the fast fluctuations will mean that the signal level is kept within a margin of a few dB. The accuracy of the compensation is in this case given by the amount of fast scintillation on the up-link signal. Errors in the attenuation estimation on the downlink due to signal noise will be greatly reduced by the low-pass filtering.

For ULPC systems which also estimate the faster signal fluctuations due to scintillation (e.g., using a separate frequency scaling procedure), additional information on the signal slope due to scintillation will be needed to assess the required tracking speed. These systems will compensate the signal level variations more accurately, however, the accuracy of the fade estimation will be limited by at least the following points: the correlation of fast scintillations on the up- and downlink at different frequencies is small [22] and the faster fluctuations will also contain more signal noise, which is uncorrelated between the up- and downlink signals.

## APPENDIX
## DETAILS ON THE DATA PROCESSING PROCEDURES AT THE DIFFERENT MEASUREMENT SITES

In **Blacksburg**, Virginia [7], propagation terminals continuously measured signals from the three Olympus beacons. The analysis 'year' consists of January–May and September–December 1991, completed by June–August 1992 to compensate for Olympus' summer holiday in 1991 [5]. Data were saved at a 10 Hz rate. Diurnal signal level variations due to spacecraft motion were removed. To alleviate sensitivity to small variations in the received signal, 10 s moving averages of attenuation were used for the fade slope, which was calculated as the difference between attenuations 5 s before and 5 s after an attenuation threshold was crossed, divided by 10 s. Fade slopes were determined for attenuation thresholds of 1, 3, 5, 10, 15, and 20 dB and sorted into bins of 0.05 dB/s wide.

In **Chilton** and **Sparsholt**, UK, [15], beacon signals from the Olympus satellite were measured and analyzed at Rutherford Appleton Laboratory. In Chilton the 29.7 GHz beacon was measured from June 1990 to May 1991 and in Sparsholt the 19.8 GHz beacon was measured from September 1992 to August 1993. The data were sampled with a time resolution of 1 Hz. Scintillation was removed from the data using a 10 s moving average LPF. The fade slope was determined at each second as the difference between attenuation (in dB) 5 s before and 5 s after the time of reference, divided by 10 s. The fade slope data were collected in conditional distributions with bin size of 1 dB for attenuation and 0.05 dB/s for the fade slope.

In **Fairbanks**, Alaska, **Tampa**, Florida and **White Sands**, New Mexico [8], signals were received from the ACTS satellite of NASA, from December 1993 to November 1995. Data were recorded at a sampling rate of 1 s. Scintillation was removed using a 100 s $\cos^2$-LPF. The fade slope was calculated as the difference between attenuation levels 5 s before and 5 s after an attenuation threshold was crossed, divided by 10 s. Fade slope statistics were classified according to fade slope value in 0.1 dB/s intervals and to attenuation value in 1 dB intervals, centered at 1, 3, 5, 10, 15, and 20 dB. As on all ACTS-sites, the antennas had a water-absorbing antenna coating, which caused extra attenuation during rain events.

In **Gometz-la-Ville** and **La-Folie-Bessin**, France [16], an Olympus measurement campaign was conducted by CNET/CETP in Paris. The 20 and 30 GHz beacons of the Olympus satellite were recorded, using a 9 m Cassegrain antenna in Gometz-la-Ville and a 1.3 m Cassegrain antenna in la-Folie-Bessin. The time resolution was 1 Hz. The measurements started at both stations in May 1992. The 30 GHz measurements continued until 12 October 1992, when this Olympus transmitter broke down. The 20 GHz measurements continued until April 1993 in La-Folie-Bessin and until the end of the satellite's operation time at 12 August 1993 in Gometz-la-Ville. The signal level data, at both frequencies, of the whole period were submitted to Onera, Toulouse, France. There, the data were low-pass filtered with a 40 s $\cos^2$-LPF. Fade slope statistics were obtained from these data using the same procedures as from the Eindhoven data.

In **La Salle**, Colorado [17], the two beacon signals of the ACTS satellite were received from January 1994 to December 1998. A 10 s moving average was applied to remove signal fluctuations due to scintillation. The fade slope was defined only if the attenuation level crossed a specified threshold and remained either larger or smaller than the threshold for more than 10 s. The fade slope for a given threshold crossing was defined as the difference between attenuation levels 5 s before and 5 s after an attenuation threshold was crossed, divided by 10 s. The fade slope was calculated for threshold values 1, 2, 3,… 31 dB and classified in bins of 0.05 dB/s wide. Also this antenna had a water-absorbing antenna coating which caused extra attenuation during rain events.

In **Lessive** and **Louvain-la-Neuve**, Belgium [18], the three Olympus satellite beacons signal levels have been measured and processed using the DAPPER software at the Université Catholique de Louvain. At Lessive, the 0 dB- level of the corresponding beacon measurements was determined from the clear-sky mean level. At Louvain, meteorological ground measurements were used for template extraction. Three months of measured and processed data from both stations, measured in July and October 1990 and March 1992, were submitted to Onera, Toulouse, France. There, the data were low-pass filtered with a sharp filter with cut-off frequency of 20 mHz. Fade slope statistics were obtained from these data using the same procedures as from the Eindhoven data.

In **Sparsholt**, UK [19], the Radio Communication Research Unit of Rutherford Appleton Laboratory measured signals from the 19, 40 and 50 GHz beacons carried on Italsat satellite F1. Attenuation along the path due to rain and clouds was estimated from the beacon signals by comparing these with clear sky levels, identified using coincident radiometer measurements. Two months of measured and processed data from Sparsholt, measured in August and October 1997, were submitted to Onera, Toulouse, France. There, the 19 GHz data were low-pass filtered with a 40 s $\cos^2$-LPF. Fade slope statistics were obtained from these data using the same procedures as from the Eindhoven data.

## ACKNOWLEDGMENT

The author wishes to thank the following persons and organizations for providing useful material for this paper: G. Brussaard, Eindhoven University of Technology, The Netherlands, for permitting the use of data measured in Eindhoven; D. Vanhoenacker, University Catholique de Louvain, Belgium, for providing data measured in Louvain-la-Neuve and Lessive; S. Ventouras, Rutherford Appleton Lab., Chilton, U.K., for providing data measured in Sparsholt; and J. Beaver, Colorado State University, Fort Collins, for sending fade slope statistics from la Salle.

## REFERENCES

[1] D. G. Sweeney and C. W. Bostian, "Implementing adaptive power control as a 30/20-GHz fade countermeasure," *IEEE Trans. Antennas Propagat.*, vol. 47, pp. 40–46, Jan. 1999.

[2] ——, "The dynamics of rain-induced fades," *IEEE Trans. Antennas Propagat.*, vol. 40, pp. 275–278, Mar. 1992.
[3] P. A. M. Buné, M. H. A. J. Herben, and J. Dijk, "Rain rate profiles obtained from the dynamic behavior of the attenuation of microwave radio signals," *Radio Sci.*, vol. 23, no. 1, pp. 13–22, 1988.
[4] E. Matricciani, "Rate of change of signal attenuation from SIRIO at 11.6 GHz," *Electron. Lett.*, vol. 17, no. 3, pp. 139–141, 1981.
[5] M. M. J. L. van de Kamp, "Climatic Radiowave propagation models for the design of satellite communication systems," Ph.D. dissertation, Eindhoven Univ. Technol., 1999.
[6] M. M. J. L. van de Kamp and G. Brussaard, "Statistical analysis of rain fade slope," in *Millennium Conference on Antennas & Propagation (AP 2000)*, vol. SP-444, Davos, Switzerland, Apr. 2000, paper 0970.
[7] W. L. Stutzman, T. Pratt, A. Safaai-Jazi, P. W. Remaklus, J. Laster, B. Nelson, and H. Ajaz, "Results from the Virginia tech propagation experiment using the Olympus satellite 12, 20 and 30 GHz beacons," *IEEE Trans. Antennas Propagat.*, vol. 43, pp. 54–62, Jan. 1995.
[8] J. Feil, L. J. Ippolito Jr., H. Helmken, C. E. Mayer, S. Horan, and R. E. Henning, "Fade slope analysis for Alaska, Florida and New Mexico ACTS propagation data at 20 and 27.5 GHz," *Proc. IEEE*, vol. 85, no. 6, pp. 926–935, 1997.
[9] J. S. Bendat and A. G. Piersol, *Random Data: Analysis and Measurement Procedures*, 2nd ed. New York: Wiley-Interscience, 1986.
[10] "Propagation Data and Prediction Methods Required for the Design of Earth-Space Telecommunication Systems," Recommendations of the ITU-R, Rec. P.618-7, 2001.
[11] T. K. P. Chung, A. P. Gallois, and B. C. Gremont, "Frequency scaling of rain attenuation: Results from Olympus satellite," in *Proc. 9th Int. Conf. Antennas and Propagation (ICAP '95), IEE Conf. Publ. 407*, vol. 2, 1995, pp. 178–181.
[12] E. Matricciani, "Effects of filtering on rate of change of rain-induced attenuation," *Electron. Lett.*, vol. 18, no. 11, pp. 477–478, 1982.
[13] T. Maseng and P. M. Bakken, "A stochastic dynamic model of rain attenuation," *IEEE Trans. Commun.*, vol. COM-29, no. 5, pp. 660–669, 1981.
[14] M. van de Kamp and P. Clérivet, "The influence of time interval and filter bandwidth on measured rain fade slope," in $4^{\grave{e}mes}$ Journées d'études 'Propagation Électromagnétique dans l'Atmosphère du Décamétrique a l'Angström', Rennes, France, Mar. 2002, Paper 63.
[15] S. Ventouras, "Fade Slope Characteristics," Rutherford Appleton Laboratory, Radio Communications Research Unit, NRPP Research Note 157, 1995.
[16] P. Golé, A. M. Ulmer-Moll, M. Vernet, and J. Lavergnat, "Les Résultats de l'Expérience OLYMPUS,", Paris, France, Technical Report NT/PAB/RGF/RCN/3826, NT/PAB/RSH/HYS/3826, NT/CETP/001, CNET/CETP, 1994.
[17] V. N. Bringi and J. Beaver, "Ka-Band propagation studies using the ACTS propagation terminal and the CSU-CHILL multiparameter radar," in *Proc. 21st NASA Propagation Experimenters Meet. (NAPEX XXI)*, El Segundo, CA, June 1997, pp. 1.47–74.
[18] H. Vasseur, I. Adams, C. Amaya, and D. Vanhoenacker, "Comparison of yearly statistics with CCIR prediction methods," in *Proc. 21st Meet. Olympus Propagation Experimenters (OPEX XXI)*, Louvain-la-Neuve, Belgium, May 1994, pp. 80–89.
[19] S. Ventouras, C. L. Wrench, and S. A. Callaghan, "New thinking required to offset limitations imposed by V-band propagation," in 19th International Communications Satellite Systems Conference and Exhibit (ICSSC-19), Toulouse, France, April 2001, paper 37.
[20] R. K. Crane, X. Wang, D. B. Westenhaver, and W. J. Vogel, "ACTS propagation experiment: Experiment design, calibration and data preparation and archival," *Proc. IEEE*, vol. 85, no. 6, pp. 863–878, 1997.
[21] F. K. Lutgens and E. J. Tarbuck, *The Atmosphere*, 7th ed. Upper Saddle River, NJ: Prentice-Hall, 1998.
[22] S. I. E. Touw and M. H. A. J. Herben, "Short-term frequency scaling of clear-sky and wet amplitude scintillation," *IEE Proc.-Microw. Antennas Propag.*, vol. 143, no. 6, pp. 521–526, 1996.

**Max M. J. L. van de Kamp** was born in Driebergen, the Netherlands, in 1963. He received the M.Sc. degree in electrical engineering in 1989 and the Ph.D. degree in telecommunications in 1999, both from Eindhoven University of Technology ('EUT'), the Netherlands.

He has been working as a Research Scientist in different radiowave propagation research projects: in 1990–1994 at EUT, in 1995–1997 at Helsinki University of Technology, Finland, in 1997–1999 again at EUT and since 2000 at Onera, Toulouse, France. His activities in these projects have been studies of rain and ice depolarization, tropospheric scintillation and dynamic aspects of rain attenuation. During his various research jobs, he has been involved in international cooperational satellite propagation research projects of the European Space Agency: the Olympus Propagation Experiment ('OPEX') from 1991 to 1994, COST255 from 1995 to 1999 and COST280 since 2001.